A model for spark ignition in a gas turbine combustor

A. Neophytou
Engineering Department
University of Cambridge
Cambridge, CB2 1PZ, UK
Email: an321@cam.ac.uk

E. Mastorakos*
Engineering Department
University of Cambridge
Cambridge, CB2 1PZ, UK
Email: em257@eng.cam.ac.uk

E. S. Richardson
Faculty of Engineering and the Environment
University of Southampton
Southampton, SO17 1BJ, UK
Email: e.s.richardson@soton.ac.uk

S. Stow
Rolls-Royce plc
Derby, UK
Email: simon.stowe@rolls-royce.com

M. Zedda
Rolls-Royce plc
Derby, UK
Email: marco.zedda@rolls-royce.com

A model that simulates the possible flame trajectories following spark ignition in a generic recirculating flame has been applied to a realistic aero-engine combustor. The model has been previously validated for gaseous and simple spray flames. It uses a CFD solution of the un-ignited flow and estimates the volume of the combustor that could be ignited given a particular flow field, spray distribution, and spark location, shape and size, and also provides a measure of the variability between independent sparking events. From this information, the ease of igniting the combustor can be assessed, and hence the combustor and injector geometry and spark placement decisions can be informed at a very early stage of the design process. Results for igniting a Rolls-Royce test combustor run with kerosene at high-altitude relight conditions for which experimental data are available and for which a RANS CFD solution has been developed, demonstrate the usefulness of the model's output. The results are consistent with experiment and also reveal that the spark characteristics and location used in the experiments, developed over a number of years by trial-and-error methods, are indeed close to optimum.

1 Introduction

Aircraft engines must satisfy high-altitude relight capability. Non-expensive models that predict the flame propagation following spark ignition are valuable in assisting engineers during the design stage of combustors. Recently, a physics-based model with low computational cost was presented in Ref. [1] and aimed at reproducing the growth of a flame following ignition in recirculating flows by interrogating a cold CFD solution. The dominant physics found by previous experiments with recirculating flows [2–5] were implemented in the model. The model reproduced the turbulent diffusion and the mean convection of the flame, the flammability limits in sprays, and the local extinction due to the turbulent strain rate [1]. In addition, the randomness of the turbulent transport of flame elements and the randomness of the local mixture fraction was incorporated. This led to different realisations of the flame growth with the same initial conditions of spark, as demonstrated in experiments [2, 3]. In Ref. [1], the ignition progress factor π_{ign}, defined as the volume of flammable mixture that has been ignited, was shown to be an interesting quantity to study and led to a calculation of the ignition probability (i.e. the probability that the whole flame will be ignited from depositing a spark at a given location), which agreed reasonably well with experimentally-determined distributions. The model therefore is in a state to be used in realistic geometries and sparks.

In this paper, the model is applied to a test kerosene combustor from Rolls-Royce that has been studied numerically [6] and experimentally [5, 7]. The statistics of π_{ign} are investigated for different spark configurations. The location and the shape of the spark, for the same spark energy, that lead to the best ignition behaviour are explored.

*Address all correspondence to this author.

Previous experimental investigations with ignition of recirculating spray flames showed that ignition was successful if the flame kernel was convected towards the fuel injector by the flow [3–5]. In addition, a parametric investigation of the spark position along the side wall of the burner in Ref. [3] demonstrated that the best axial location was at the maximum width of the central recirculation zone. Experiments done with the combustor investigated here showed that ignition has a probabilistic nature, that the time between ignition and overall flame stabilisation varies between 30 ms and 50 ms, and that successful ignition is associated with a kernel that moved upstream [7]. The two last findings were also reported in a LES simulation presented in Ref. [6]. The model used in this study intends to reproduce these findings.

Firstly, we introduce the mathematical model and the combustor investigated. Then we present results computed with the model. The paper concludes on the potential of the model in assisting the design of combustion chambers.

2 Numerical formulation

The model was described in detail in Ref. [1], where a detailed comparison with experimental data on spark ignition with gaseous and spray flames in simple geometries is given. In this section, the main concepts of the model are repeated for clarity and the CFD solution of the combustor are briefly presented.

2.1 Model description: main idea

The model aims at representing the possible trajectories of individual flame elements originating from a spark in a generic flow field carrying droplets. A time-averaged CFD solution of the cold flow is needed as an input for the model. The present model is based on the following rules:

1. The flow is filled with regular "grid cells" with an arbitrary size. These grid cells can have two states, cold or burnt. Initially, all grid cells are in the cold state. Cells are placed throughout the combustor volume.
2. The simulation is initialised by defining a spark volume in the domain. All grid cells that overlap with the spark volume are switched to the burnt state and each of them releases a "flame particle". Any shape of spark can be used.
3. A flame particle is tracked with a Langevin model using the cold CFD field. A particle can extinguish according to a criterion based on a Karlovitz number, presented below. When a particle extinguishes, it is no longer computed.
4. Every time a particle visits a grid cell in a cold state, the grid cell switches to the burnt state and a new particle is emitted at its center and follows its own random walk.
5. Throughout the simulation, the number of cells in a burnt state divided by the total number of cells is computed as a function of time. This ratio is named "ignition progress factor" and is given the symbol π_{ign}.
6. The computation is repeated many times with different realisations. The statistics of π_{ign} for this spark location can be analysed to assess ignition performance.

By repeating this procedure for different spark locations, spark shapes etc, and comparing the resulting statistics of π_{ign}, the relative performance of the various sparks and of their placement can be assessed. "Good" ignition implies high values of π_{ign} at the end of the simulation, while "bad" ignition implies a low value, since the flame would not have traveled much before it is either extinguished or convected out of the combustor. Very repeatable behaviour implies that every realisation gives similarly "good" or "bad" ignition characteristics, i.e. low $\pi_{ign,rms}$, while a spark or a particular spark location giving very variable ignition behaviour would be characterised by high $\pi_{ign,rms}$. The usefulness of the resulting values of π_{ign} lies more in relative comparisons, than in absolute values.

2.2 Mathematical formulation

The particle position in direction i evolves according to the stochastic differential equation:

$$dX_{p,i} = U_{p,i}dt \tag{1}$$

where $U_{p,i}$ is the particle velocity in direction i. $U_{p,i}$ follows the simplified Langevin model [8] and consists of a linear drift towards the local Favre averaged velocity of the flow and an added isotropic diffusion term:

$$dU_{p,i} = -(\frac{1}{2}+\frac{3}{4}C_0)\omega_p(U_{p,i}-\widetilde{U}_i)dt + (C_0\varepsilon_p dt)^{1/2}N_{p,i} \tag{2}$$

where $\widetilde{U}_i$ is the local Favre averaged velocity in direction i, $N_{p,i}$ is a normally distributed variable (with mean zero and variance unity), C_0 is a constant assumed equal to 2.0 [8], ε_p is the turbulent dissipation at the particle location and ω_p is the inverse turbulent timescale at the particle location $\omega_p = u'_p/L_{turb,p}$, $u'_p = (2/3k_p)^{1/2}$ with k_p the local turbulent kinetic energy and $\varepsilon_p = k_p\omega_p$. The random variable $N_{p,i}$ for one particle is independent from another (the velocity correlation between particles is ignored). Hence, particles are simply convected by the turbulent flow and undergo random walk to model their dispersion.

At the end of each time step, a criterion based on a Karlovitz number is used to assess if the particle extinguishes. A Karlovitz number Ka_p is defined for each particle and is compared to a critical value Ka_{crit}. If $Ka_p > Ka_{crit}$, the particle extinguishes. Ka_p is defined as the ratio between the chemical time and the reciprocal eddy lifetime [9]:

$$Ka_p = 0.157\left(\nu\frac{(u'_p)^3}{L_{turb,p}}\right)^{1/2}\frac{1}{S^2_{L,p}} \tag{3}$$

where ν is the mixture kinematic viscosity, taken as $1.57\times 10^{-5}m^2/s$ and $S_{L,p}$ is the laminar flame speed, detailed below. The critical value Ka_{crit} was found by Abdel-Gayed and Bradley to be 1.5 for premixed flows [9].

The stochastic differential equation for the mixture fraction of a particle assuming interaction by exchange with the mean [8], and applying the mean evaporation rate from the local CFD cell, is given by:

$$d\xi_p = -\frac{1}{2}C_\xi \omega(\xi_p - \widetilde{\xi})dt + (1-\widetilde{\xi})\frac{\bar{\Gamma}_m}{\bar{\rho}}dt \qquad (4)$$

where D is the fuel mass diffusivity, ρ is the local flow density while Γ_m is the mass source term due to evaporation, ξ_p is the particle mixture fraction and $\widetilde{\xi}$ is the local Favre averaged mixture fraction of the flow. C_ξ is a constant taken equal to 2.0 [8]. The advancement of ξ_p enables the calculation of $S_{L,p}$ in a pure gas and in turn of Ka_p. The computation of $S_{L,p}$ in a spray is presented in Section 2.3.

The initial velocity of each particle is a random Gaussian variable with a rms equal to the local turbulent intensity. The initial mixture fraction of each particle follows a beta pdf with mean and rms coming from the local CFD solution. Different realisations are obtained by setting different random distributions.

2.3 Laminar flame speed calculation

The value of S_L is needed for the evaluation of the local Karlovitz number of the particle. S_L must be given for sprays as a function of overall equivalence ratio ϕ_0 (i.e. using both the gaseous fuel vapour and the liquid fuel), the vapour fraction Ω and the droplet diameter a_d. Such information can be provided experimentally or numerically. For the case of altitude relight, we need S_L at low pressure and low temperature conditions. Calculations of laminar spray premixed flames that can provide the S_L needed have been performed already [10]. The results were correlated by:

$$S_L = S_{L,max}\frac{2.5}{\sqrt{2\pi}}\exp\left(-\frac{(\phi_0-\mu)^2}{2\sigma^2}\right) \qquad (5)$$

The flame speed is determined by the three parameters $S_{L,max}$, μ and σ. $S_{L,0}$ is the gaseous laminar flame speed at stoichiometry, $\mu_g = 1.07$ and $\sigma_g = 0.33$. If $\phi_0 \leq 0.5$, the flame speed is set to zero. For very small droplets $a_d \leq 5\mu m$, we assume that the spray flame speed is identical to the gaseous one, $S_{L,max} = S_{Lg,max}$, $\mu = \mu_g$ and $\sigma = \sigma_g$. For pure gas, $S_{Lg,max} = 1.01 S_{L,0}$.

For larger droplets $a_d > 5\mu m$, we use the following expressions:
For n-decane at atmospheric conditions:

$$\begin{aligned} S_{L,max}(\Omega=0)/S_{L,0} &= -0.0090(\ln(a_d))^3 \\ -0.430(\ln(a_d))^2 - &\quad 6.287(\ln(a_d)) - 28.051 \\ \mu(\Omega=0) &= -0.642(\ln(a_d))^3 \\ -20.231(\ln(a_d))^2 - &\quad 208.844(\ln(a_d)) - 702.263 \\ \sigma(\Omega=0) &= -0.412(\ln(a_d))^3 \\ -12.994(\ln(a_d))^2 - &\quad 134.428(\ln(a_d)) - 453.188 \end{aligned} \qquad (6)$$

For n-decane at high altitude relight conditions (P_0=41.37 kPa, T_0=265 K):

$$\begin{aligned} S_{L,max}(\Omega=0)/S_{L,0} &= -0.0224(\ln(a_d))^3 \\ -0.859(\ln(a_d))^2 - &\quad 10.840(\ln(a_d)) - 44.035 \\ \mu(\Omega=0) &= -0.974(\ln(a_d))^3 \\ -30.892(\ln(a_d))^2 - &\quad 322.963(\ln(a_d)) + 1109.328 \\ \sigma(\Omega=0) &= -0.566(\ln(a_d))^3 \\ -17.765(\ln(a_d))^2 - &\quad 183.279(\ln(a_d)) - 619.262 \end{aligned} \qquad (7)$$

The coefficients vary linearly between their value at $\Omega = 0$ to their value at $\Omega = 1$ (pure gas):

$$S_{L,max} = (S_{Lg,max} - S_{L,max}(\Omega=0))\Omega + S_{L,max}(\Omega=0) \qquad (8)$$

$$\mu = (\mu_g - \mu(\Omega=0))\Omega + \mu(\Omega=0) \qquad (9)$$

$$\sigma = (\sigma_g - \sigma(\Omega=0))\Omega + \sigma(\Omega=0) \qquad (10)$$

Note that the data for n-decane can be used instead of kerosene, which is the fuel of relevance to aviation gas turbines, as the two fuels have reasonably similar flame speeds [11]. Note also that the laminar flame simulations [10] show very small changes in the flame speed between atmospheric and relight conditions, possibly due to the detrimental effect of the low temperature being balanced by the beneficial effect of the low pressure.

The CFD solution (presented later) includes spray, and so the Sauter Mean Diameter (SMD), the fuel vapour and the fuel in liquid phase are available at every grid node, and hence S_L at every grid node from the above correlation can be calculated.

2.4 Combustor investigated and model settings

The combustion chamber is shown in Fig. 1a. The downstream direction is aligned with the x-axis. The high-altitude test rig is a two-sector rig, one sector (the left-hand sector when looking downstream) being fitted with a lean-burn injector (Rolls-Royce Deutschland Ltd & Co KG), and the other having an un-fuelled dummy injector. The fuel injected is liquid kerosene. A RANS solution of a cold flow field of this geometry was performed in Rolls-Royce laboratories using the in-house code PRECISE (see [6] and references therein). The operating conditions chosen for modelling in the CFD calculations are given in Table 1. The RANS solution provides the three components of the mean velocity, the turbulent kinetic energy and dissipation rate, the fuel and liquid fuel mass fractions, and the Sauter Mean Diameter at every CFD grid cell.

The flame particle tracking is performed on a rectangular Cartesian grid (which can be larger than the CFD domain). Each of these cells is initially deemed "cold". The time step in the flame particle tracking is $dt = 0.5$ ms, lower than the estimated turbulent timescale $L_{turb}/u' = 2$ ms in the flow. The simulations stops after 60 ms, which has been

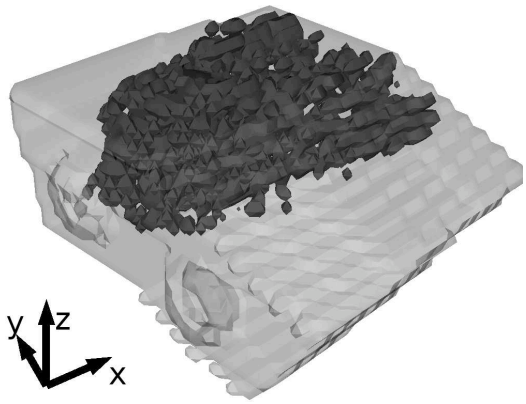

(a)

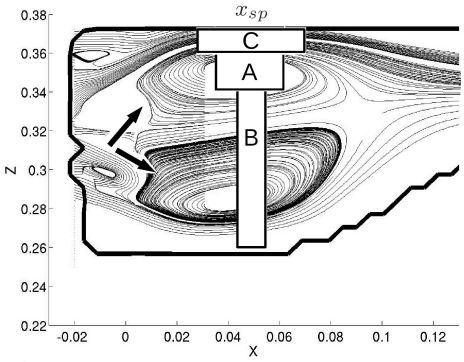

(b)

Fig. 1. (a) Geometry of the test combustor [6]. The black iso-surface shows qualitatively the fuel mass fraction. (b) Plane $y = 0$ mm contains the axis of the cylindrical sparks studied. The two arrows show qualitatively the spray angle. The shapes of sparks A, B and C are represented. In the figure, the axis of the spark is at $x_{sp} = 47.5$ mm.

found to be long enough for the flame particles to have experienced all their possible histories.

The value of $(C_0\varepsilon_p dt)$ is estimated from the average turbulent dissipation rate in the domain (about 19000 m^2/s^3). The number of grid cells was 672,287, while the spacing was equal to $2(C_0\varepsilon_p dt)^{1/2}dt$, which resulted in a grid size of 2 mm. The quantity $2(C_0\varepsilon_p dt)^{1/2}dt$ is the maximum spacing for the grid used for tracking the flame, as suggested in Ref. [1]. 50 independent spark events were simulated. Under those conditions, the CPU time to compute a single spark event was about 30 min in a desktop PC.

The different sparks studied are summarised in Table 2. All sparks investigated are cylindrical, the cylinder axis being aligned with the z-axis, and have the same volume (i.e. same energy). Sparks are located on the upper wall on the line $y = 0$ mm and a parametric investigation is carried out on the spark shape (length L_{sp} and diameter d_{sp} of the cylinder), and the location of the spark axis x_{sp}. The sparks studied are illustrated in Fig. 1b.

At $t = 0$, all model grid cells intersecting the spark are deemed "burnt" and a random walk of the flame particles starts from each of these burnt cells. Large sparks, therefore, emit more flame particles than small sparks.

Table 1. Operating conditions used in the CFD RANS simulation.

Air pressure (bar)	0.552
Air temperature (K)	278
Fuel temperature (K)	288
Normalized air mass flow	0.38
Normalized fuel-air ratio	0.56

Table 2. Different cases studied in the simulations (spark position along centerline x_{sp}, spark diameter d_{sp}, spark length L_{sp}).

Spark	x_{sp} (mm)	L_{sp} (mm)	d_{sp} (mm)
A	[0,100]	27.9	28
B	47.5	12.4	42
C	47.5	111.6	14

3 Results

3.1 Effect of spark location

Figure 2a shows the time evolution of π_{ign} for all events for spark A at $x_{sp} = 0.475m$. In all events, π_{ign} slowly increases until $t = 10$ ms, then rapidly increases until $t = 40$ ms and finally stabilises to a constant value. The simulations reproduce the stochasticity of ignition since each event results in different values of π_{ign}. In addition, the timescale over which the increase of π_{ign} occurs is about 50 ms. This is close to the ignition timescale reported by the experiment [7] and the LES simulation of Ref. [6]. Considering the values of π_{ign} for each event at the end of the simulation, i.e. $t = 60$ ms, a mean and a rms can be calculated, see Fig. 2a. These two quantities reveal the mean amount of burned material and the variability of ignition associated with the particular spark center and the spark shape. In Fig. 2a, the average and the rms of π_{ign} are respectively 0.19 and 0.006. The low value of the rms suggests that different events lead to fairly similar final values of burned volume.

Figure 3 shows the evolution of the mean and the rms of π_{ign} with x_{sp} for spark A. It is evident that the mean of π_{ign} first increases with x_{sp}, stabilises to a relatively high value in the range 20 mm $< x_{sp} \leq 50$ mm, then decreases with x_{sp} and stabilises to a relatively low value in the range 80 mm $< x_{sp} \leq 100$ mm.

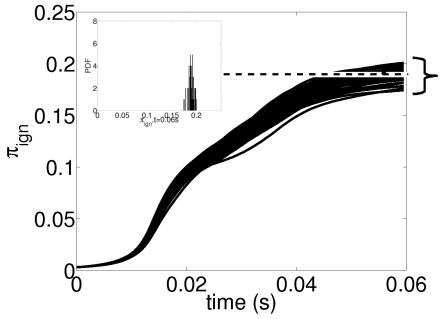

(a)

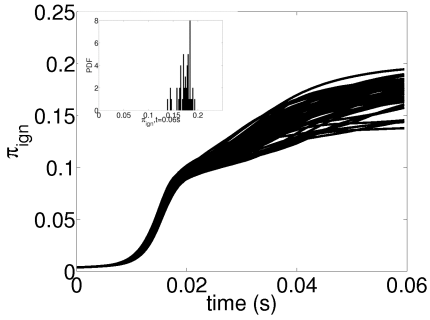

(b)

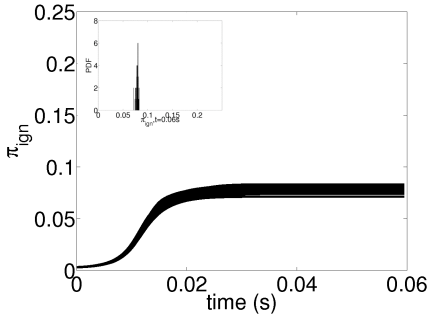

(c)

Fig. 2. Time evolution of π_{ign} of each event with $x_{sp} = 47.5$ mm for (a) spark A, (b) spark B and (c) spark C. On the top left of the figures is the PDF of π_{ign} at the end of the simulation. In (a) the dashed line and the bracket show respectively the average and the range of π_{ign} at the end of the simulation.

Close to the injector, 0 mm $< x_{sp} \leq 20$ mm, the spark is located in a region upstream of the recirculation zone, in the corner, see Fig. 1b. The low value of the average of π_{ign} at $x_{sp} = 0$ mm indicates that in most cases, the flame does not spread and rapidly extinguishes. In addition, the high rms of π_{ign} shows that ignition there is very probabilistic and that in some events, a large volume is ignited while in others the kernel rapidly extinguishes. In this zone, there is virtually no fuel. However, due to the large spark size, some

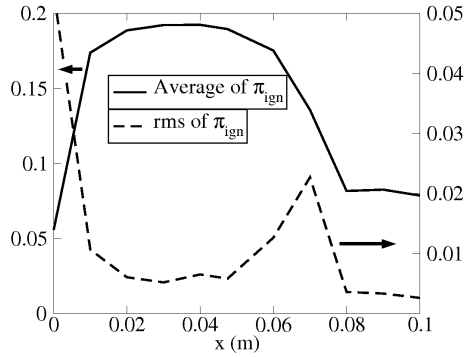

Fig. 3. Average and rms of π_{ign} computed at the end of the simulation over all events *vs.* x_{sp}.

flammable material is ignited, albeit very few. Moreover, the mean convection there is positive while the turbulent kinetic energy and the turbulent dissipation are relatively high. Therefore, the ignited particles can either be brought downstream to meet ignite regions with more fuel or they can be transported upstream where there is no fuel leading to extinction. Hence, different realisations can lead to successful ignition events or to quickly quenched kernels.

As the spark center x_{sp} increases from 0 mm to 20 mm, the average of π_{ign} increases to 0.19 while its rms decreases to 0.005. This means that for a spark at x_{sp}=20 mm, most of the events ignite a relatively large volume with a low variability. This is because there is a great overlap between the spark and the recirculation zone, see Fig. 1b. In the recirculation zone more fuel exists and ignited flame particles are easily captured by the recirculating flow and brought to the flammable region, as suggested by the experiments with recirculating sprays of Ref. [3]. This behaviour is described in greater detail in Section 3.3. In the region 20 mm $< x_{sp} \leq 50$ mm, the average and the rms of π_{ign} remain almost constant. This implies that any spark in this region will have similar ignition performance, while the low rms implies that all events lead to a relatively large volume of the burner ignited with little differences between them. Note that this region corresponds to the maximum width of the recirculation zone. In Ref. [3], the best spark placement along the axis on the side wall corresponded to the maximum width of the recirculation zone. That recommendation seems to have been reproduced by the present model applied to realistic combustors.

In the region 50 mm $< x_{sp} \leq 80$ mm, the average of π_{ign} decreases with x_{sp} while its rms first increases with x_{sp}, reaches a peak at $x_{sp} = 70$ mm and then decreases to a relatively low value. As x_{sp} increases from 50 mm, the spark center moves further away from the maximum width of the recirculation zone and in turn the overlap between the spark and the recirculation zone is less, see Fig. 1b. Therefore, the ignited flame particles are more likely to be convected downstream by the mean flow although the random turbulent motion can still bring them towards the recirculation zone. It is thus expected that the mean π_{ign} becomes lower with x_{sp}. The increase of the rms of π_{ign} is due to the increased variability. In some events all particles are convected

downstream, leading to a low π_{ign} while in others turbulence moves flame particles in the recirculation zone, leading to a high π_{ign}. The location $x_{sp} = 80$ mm corresponds to the stagnation point of the recirculation zone, see Fig. 1b. Beyond this value, there is no overlap between the spark and the recirculation zone and there is little chance that the turbulent motion brings the ignited particles in the recirculation zone. The ignited flame particles are all convected downstream and never make it to the recirculation zone. Hence, they can only ignite material on their way downstream but not upstream. This leads to a low average of π_{ign} and a low rms of π_{ign} (little variability). This behaviour is shown more in detail in Section 3.3.

3.2 Effect of spark shape

In this section, the spark center is fixed at $x_{sp} = 47.5$ mm and the statistics of the flames are compared between sparks A, B and C. Note that this spark center is in the best ignition region as shown in the previous section. Figures 2a, b and c show the evolution of π_{ign} with time for all events, respectively for spark A, B and C. Events for spark A and B both lead to relatively high values of π_{ign}. However, the variability is larger with spark B (thin and long) than with spark A. In addition, it is clear that spark C (wide and short) results in very low values of π_{ign} with all events behaving in the same way.

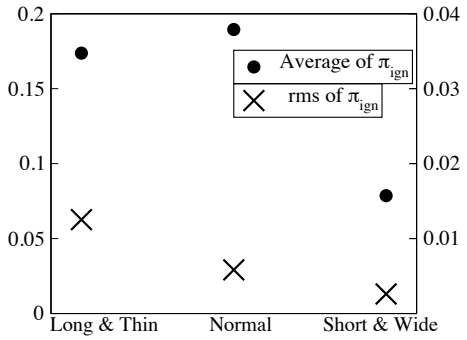

Fig. 4. Average and rms of π_{ign} computed at the end of the simulation over all events with $x_{sp} = 47.5$ mm for spark A, B and C.

Figure 4 shows the average and the rms of π_{ign} calculated over all events at the end of the simulation for sparks A, B and C. Spark A leads to the highest value of the average of π_{ign} and a low value of the rms. Spark B has a slightly lower mean and a higher rms. Thus, events in spark A repeatedly ignite a relatively large volume of the combustor while spark B does not. The behaviour of spark A is thus preferred for successful ignition. In the present combustor, the overall equivalence ratio is much higher on the sides of the recirculation zone than in the center (not shown in details here). Since in spark A, the spark volume is concentrated to a region of high equivalence ratio, more particles sample flammable mixtures than in spark B, where a substantial part of the spark is in the center of the recirculation zone where there is almost no fuel. The larger mass of flammable material ignited by spark A can then spread and ignite further material. This leads to higher π_{ign}. Moreover, it is possible that since spark B experiences a larger range of mean velocities and turbulence intensities than spark A, see Fig. 1b, the variability and in turn the rms of π_{ign} is higher for spark B.

With spark C, the mean and the rms of π_{ign} are both low. This implies that little material is ignited in all events. This is attributed to the shape of the spark that results in little penetration in the recirculation zone, see Fig. 1b. Although the spark overlaps with flammable material, the flow tends to convect all ignited particles downstream.

Spark A is the one used in the experiments. Its location was selected empirically to provide good ignition characteristics, while its size (length and diameter) has been approximately determined from images of the flame kernel immediately following the energy deposition. Spark A is, empirically, leading to "good" ignition. It is interesting to note that this spark and this location was also found by the model to give the best ignition performance.

3.3 Visualisation of ignition events

In this section, we show the evolution of flame particles with spark A for two different events. In the first event, $x_{sp} = 47.5$ mm and a relatively large volume of the burner is ignited. In the second event, the spark is further downstream $x_{sp} = 100$ mm and much less material is ignited. These two spark locations are representative of the best location for ignition and a bad placement of the spark, respectively. Figures 5 and 6 show the evolution of the computed particles for the first and the second event respectively.

In Fig. 5, some particles are convected downstream just after ignition. On their path out of the combustor, they ignite many grid cells, and hence many more particles are emitted. Moreover, some particles from the spark are brought towards the recirculation zone where they ignite further grid cells. The ignition occurring in the recirculation zone contributes to a large extent to the large value of π_{ign} achieved here, see Fig. 3. In contrast, Fig. 6 shows that in the second event, all particles are convected downstream. They ignite only grid cells on their path away from the injector, which leads to low values of π_{ign}.

Hence, the two present simulations show that π_{ign} is high when flame particles are convected upstream by the recirculating turbulent flow. This is consistent with the finding that ignition with this combustor is successful when the kernel moves upstream towards the fuel injector [7]. This also agrees with previous findings with recirculating combustors where ignition occurred when the spark kernel was convected by the gas towards the fuel injector [3,4].

4 Conclusions

A model, developed to calculate the flame spread following the generation of a kernel given a cold CFD solution, has been applied to a realistic aero-engine kerosene combustion chamber. A parametric study on the characteristics

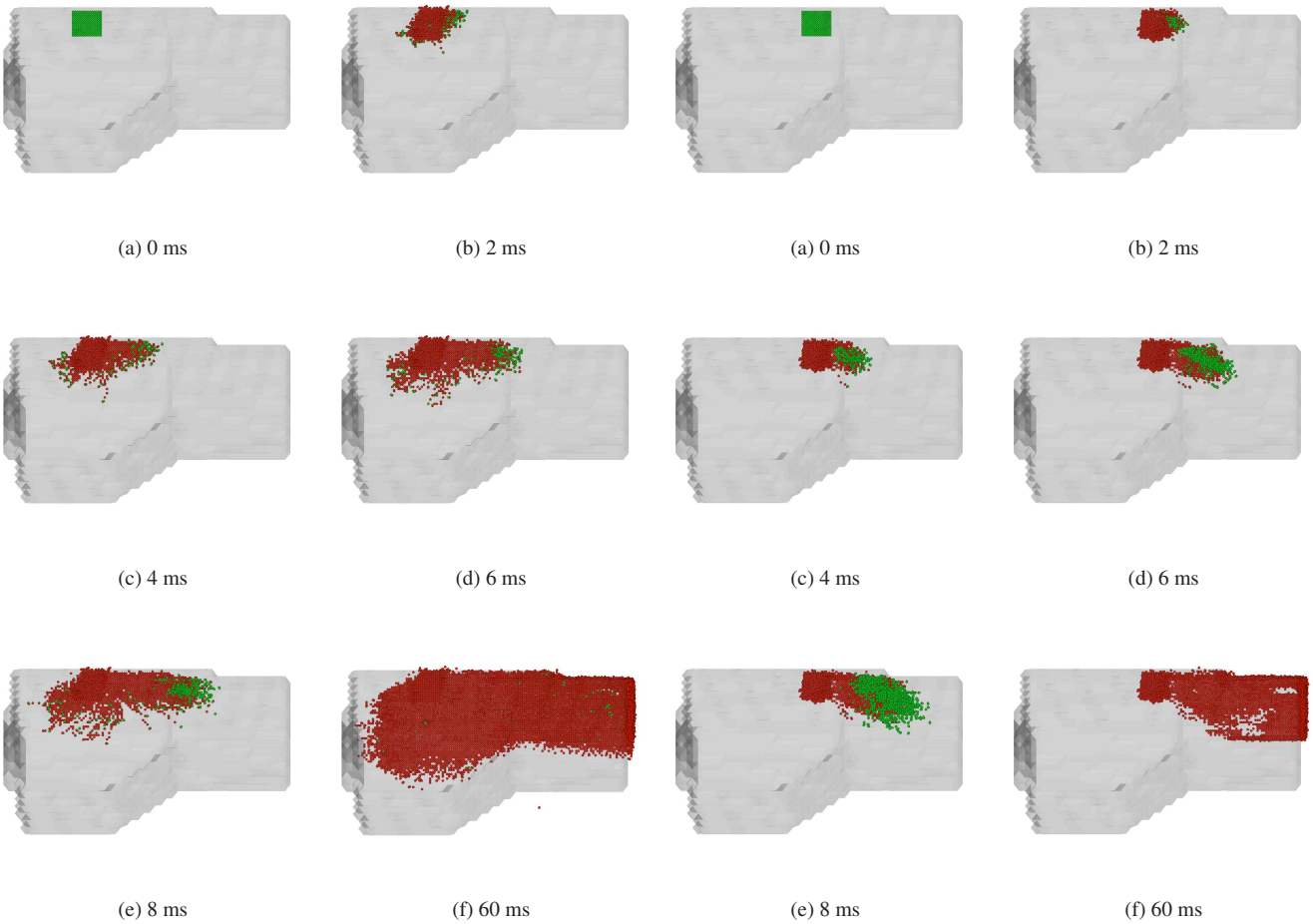

(a) 0 ms (b) 2 ms (c) 4 ms (d) 6 ms (e) 8 ms (f) 60 ms

Fig. 5. Evolution of particles with spark A, good ignition event (x_{sp}=47.5 mm), between t=0 ms and t=60 ms. Green spheres represent particles are those that are in motion (i.e. have $Ka < Ka_{crit}$). Red spheres represent extinguished particles ($Ka > Ka_{crit}$).

(a) 0 ms (b) 2 ms (c) 4 ms (d) 6 ms (e) 8 ms (f) 60 ms

Fig. 6. Evolution of particles with spark A, poor ignition event (x_{sp}=100 mm), between t=0 ms and t=60 ms. Green spheres represent particles are those that are still in motion (i.e. have $Ka < Ka_{crit}$). Red spheres represent extinguished particles ($Ka > Ka_{crit}$).

and location of the cylindrical spark was performed by varying the location of the spark center x_{sp}, the spark length L_{sp} and the spark diameter d_{sp}. For each configuration, 50 spark events were calculated and statistics on the ignition progress factor π_{ign}, i.e. the relative volume of the burner that has ignited, were compiled.

The simulation reproduced the stochastic nature of ignition and the timescale for the flame spread, the former in qualitative and the latter in quantitative agreement with experiment [7]. Furthermore, high values of π_{ign} were associated with flame particles moving towards the injector, consistent with the experiments [7] and previous work on recirculating spray flames [3,4]. The region of best spark location was shown to be at the maximum width of the recirculation zone, in agreement with experiments on an academic burner [3]. Moreover, the optimum spark shape was suggested to be a spark volume that has a great overlap with the side of the recirculation zone, where the mixture is flammable and the recirculating flow captures the flame. It is interesting to note that the spark location that gives the best ignition performance according to the model is the one selected for the experiment after years of practical experience.

This model is relevant to study the ignition process in aero-engine combustors. Since the simulations are relatively cheap, the model can also be used to carry out parametric investigations of ignition, e.g. with different spark positions, air flow rate, or fuel-air ratio, provided a reliable CFD solution of the un-ignited flow is available.

Achnowledgements

The work at the University of Cambridge has been funded by the Rolls-Royce Group and the European Commission through project TECC-AE (ACP7-GA-2008-211843). The work in Rolls-Royce has been funded by the European Commission through project TIMECOP-AE (AST5- CT-2006-030828). The paper reflects only the authors views and the Community is not liable for any use that may be made of the information contained therein.

References

[1] Neophytou, A., Richardson, E. S., and Mastorakos, E.“, 2010.”. *Combust. Flame*. Submitted for publication.

[2] Ahmed, S. F., Balachandran, R., Marchione, T., and Mastorakos, E.“, 2007.”. *Combust. Flame,* **151**, pp. 366–385.

[3] Marchione, T., Ahmed, S. F., and Mastorakos, E.“, 2009.”. *Combust. Flame,* **156**, pp. 166–180.

[4] Read, R. W., Rogerson, J. W., and Hochgreb, S., 2010. “Flame imaging of gas turbine relight”. *AIAA Journal,* **48**, pp. 1916–1927.

[5] Mosbach, T., Sadanandan, R., Meier, W., and Eggels, R. L. G. M., 2010. “Experimental Analysis of Altitude Relight Under Realistic Conditions Using Laser and High-Speed Video Techniques”. *In: Proc. ASME Turbo Expo 2010, Glasgow, UK, 14 - 18 June*.

[6] Stow, S., Zedda, M., Triantaffylidis, A., Garmory, A., Mastorakos, E., and Mosbach, T., 2011. “Conditional Moment Closure LES modelling of an aero-engine combustor at relight conditions”. *In: ASME Turbo Expo 2011, Vancouver, Canada, 6 - 10 June*. Paper GT2011-45100.

[7] Mosbach, T., Sadanandan, R., and Meier, W., 2009. “Report on the Results of Measurement Campaigns at RR-Rig”. *Deliverable D2.2.3a, EU Project No. AST5-CT-2006-030828*.

[8] Pope, S. B., 2000. *Turbulent Flows*. Cambridge University Press, London.

[9] Abdel-Gayed, R. G., and Bradley, D.“, 1985.”. *Combust. Flame,* **62**, pp. 61–68.

[10] Neophytou, A., and Mastorakos, E.“, 2009.”. *Combust. Flame,* **156**, pp. 1627–1640.

[11] Franzelli, B., Riber, E., Sanjose, M., and Poinsot, T.“, 2010.”. *Combust. Flame,* **157**, pp. 1364–1373.